Journal of Solid State Chemistry **168,** 184–191 (2002)
doi:10.1006/jssc.2002.9708

Pressure-Induced Structural Deformations in SeO_2

A. Grzechnik,*[,1] L. Farina,*[,2] R. Lauck,* K. Syassen,* I. Loa,* and P. Bouvier†

*Max-Planck-Institut für Festkörperforschung, Heisenbergstr. 1, D-70569 Stuttgart, Germany; and †European Synchrotron Radiation Facility, B.P. 220, F-38000 Grenoble Cedex, France

Received March 15, 2002; in revised form June 4, 2002; accepted July 16, 2002

The high-pressure behavior of low-dimensional selenium dioxide SeO_2 ($P4_2/mbc$, $Z = 8$) is studied with Raman scattering and synchrotron angle-dispersive X-ray powder diffraction in a diamond anvil cell up to 23 GPa at room temperature. Pressure-induced transformations in this material involve a sequence of structural distortions of the chain structure. The transformation occuring above 7.0 GPa is due to symmetry lowering to space group *Pbam* ($Z = 8$) without major changes of the crystal lattice dimensions and coordination around the Se atoms. Like in the ambient pressure polymorph, the structural unit is a SeO_3E polyhedron, where E is a Se non-bonded electron lone pair, or an irregular tetrahedron with the O atoms and Se lone pair at the vertices. Further structural transitions above 17 GPa are likely to be the result of additional distortions leading to monoclinic symmetry of the crystal structure. All transformations are reversible with little hysteresis.

Key Words: **synchrotron angle-dispersive powder X-ray diffraction; Raman spectroscopy; crystal structure; low-dimensional solids; non-bonded electron lone pair; selenium dioxide.**

INTRODUCTION

Selenium dioxide SeO_2 belongs to a family of compounds in which the stereochemical effect of non-bonded electron lone pairs results in strong asymmetry of coordination polyhedra (1). The structure of SeO_2 at ambient conditions ($P4_2/mbc$, $Z = 8$) is built of infinite puckered chains of corner-sharing SeO_3E structural units along the c-axis (Fig. 1), where E is a Se lone pair (2). The Se atom is bonded to three oxygen atoms to form a SeO_3 pyramid or an irregular tetrahedron with the O atoms and Se lone pair at the vertices. When the next-nearest oxygen atoms of the adjacent chains are considered, the Se–O coordination can be described as a distorted octahedron.

Many oxide materials built of asymmetric coordination units are non-centrosymmetric with nonlinear optical properties (3). They are often synthesized from simple oxides containing cations with non-bonded electron pairs. In this respect, the best example is the system Te–Se–O_2 (3–6), in which several phases have second-harmonic-generating (SHG) properties. SHG efficiences of some of the Te–Se oxides are two orders of magnitude higher than that of SiO_2 (6). In addition, low-dimensional solids are obtained when oxides containing lone pair elements are mixed with transition metal oxides, e.g., the SeO_2–V_2O_5 system (7).

The effect of pressure on the stereochemistry of electron lone pair elements has not been extensively studied. One could speculate on the possibility of pressure-induced phase transitions in the relevant compounds leading to changes of structure dimensionality, centrosymmetry-to-non-centrosymmetry transformations, or to the synthesis of new materials with compositions not obtainable at atmospheric conditions. In this study, we are concerned with the high-pressure behavior of one-dimensional SeO_2 studied with Raman spectroscopy and angle-dispersive powder X-ray diffraction in a diamond anvil cell above 20 GPa at room temperature. SeO_2 is a basic component of several oxide systems with low-dimensional structures and/or with nonlinear optical properties. The knowledge of the pressure effect on its bonding and dimensionality would be helpful in understanding pressure-induced phenomena in more complex systems based on SeO_2. Recent investigations of selenium dioxide with Raman spectroscopy up to 10 GPa showed no clear evidence for a structural phase transition (8). Instead, we find a sequence of structural distortions in the chain structure of SeO_2 with an onset at about 7.0–8.0 GPa. The new high-pressure phases are structurally related to the one stable at ambient pressure (2). We discuss our observations in relation to other compounds containing cations with electron lone pairs.

[1] To whom correspondence should be addressed. Fax: +49-711-689-1010. E-mail: andrzej@servix.mpi-stuttgart.mpg.de.

[2] Permanent address: Dipartimento di Chimica Fisica e Inorganica, Università di Bologna, Viale Risorgimento 4, I-40136 Bologna, Italy.

0022-4596/02 $35.00

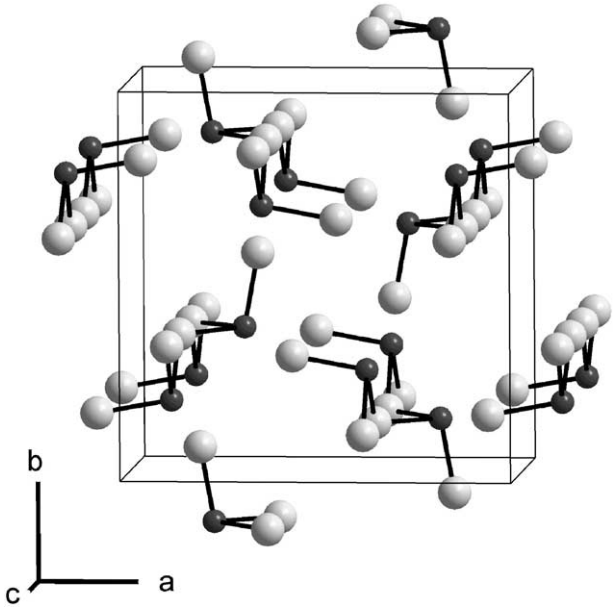

FIG. 1. Crystal structure of SeO_2 at ambient pressure (2). Dark and light symbols represent the Se and O atoms.

EXPERIMENTAL

Crystals of SeO_2 were grown by a vapor synthesis reaction, in which selenium was sublimated in an oxygen atmosphere at about 600 K at an initial pressure of 500 mbar. With a temperature gradient of about 17 K/cm, needle-like crystals of selenium and SeO_2 with a length up to 5 mm were obtained at about 500 and 400 K, respectively, after 16 days. The colorless crystals were gently ground into a polycrystalline material for further investigations at high pressures. Such a sample was investigated with Raman spectroscopy in a closed diamond anvil cell. It appeared to be of a pure SeO_2 composition (9) without any traces of H_2SeO_3 (10) that forms instantly upon exposing the SeO_2 sample to moisture. During loading into a diamond cell, the sample was always handled in a glove box in an atmosphere of dry nitrogen. The sensitivity of SeO_2 towards moisture precluded any use of a pressure medium for all the measurements.

Raman spectra at high pressures were collected using a triple spectrograph (1800 groove/mm gratings) with CCD signal detection. Raman scattering was excited with an Ar^+ laser at a wavelength of 514.5 nm. The laser power was less than 10 mW to avoid any thermal damage of the sample. Angle-dispersive powder X-ray diffractograms were measured at the ID30 beamline of the European Synchrotron Radiation Facility, Grenoble. Monochromatic radiation at a wavelength of 0.3738 Å was used for pattern collection on image plates. The images were integrated using the program FIT2D (11) to yield intensity versus 2θ diagrams. The ruby luminescence method (12) was used for pressure calibration.

RESULTS AND DISCUSSION

Raman Spectroscopy

SeO_2 crystals are centrosymmetric, whose unit cell contains eight formula units ($D_{4h}^{13}, Z = 8$). The vibrational modes are distributed as $\Gamma_{\text{vibr.}} = 5A_{1g} + 6A_{2g} + 6B_{1g} + 5B_{2g} + 7E_g + 3A_{1u} + 3A_{2u} + 4B_{1u} + 3B_{2u} + 10E_u$, where the A_{1g}, B_{1g}, B_{2g}, and E_g modes are Raman active, while the A_{2u} and E_u modes are infrared active. The factor group analysis and assignment of the vibrational modes are fully described elsewhere (9). Selected Raman spectra of SeO_2 upon compression up to 20 GPa are shown in Fig. 2. We observed 20 of the 23 predicted Raman bands ($5A_{1g} + 6B_{1g} + 5B_{2g} + 7E_g$) in our spectra (Table 1). The three missing modes are weak features that are only observed at low temperatures and atmospheric pressure (9).

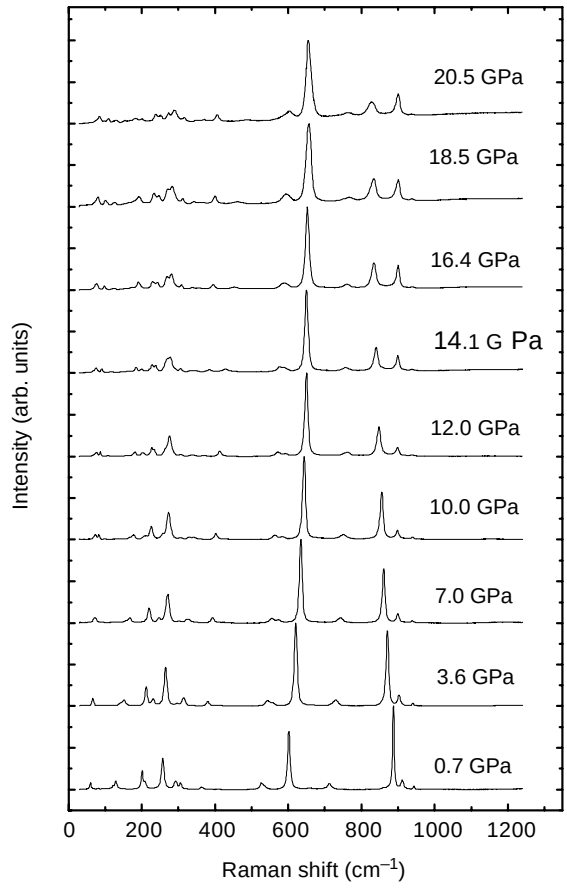

FIG. 2. Selected Raman spectra of SeO_2 upon compression.

TABLE 1
Observed Raman Frequencies ω in cm^{-1} in SeO_2 at 15 K and 10^{-4} GPa (9) and at 298 K and 0.05 GPa

Mode	ω (15 K) Ref. (9)	Type of mode	ω (298 K, 0.05 GPa) This work	$d\omega/P$ This work	$d\omega/dP$ Ref. (8)
B_{2g}	49.4	Chain translation	55.2	1.6	
E_g	53.4		58.3	1.6	1.1
A_{1g}	60.7		62.3	4.4	
	101.3	Chain deformation			
B_{1g}	118.0		119.1	7.1	
B_{2g}	131.8		126.4	7.1	4.0
E_g	197.5	Intrachain O–Se–O bending	199.5	2.9	2.3
A_{1g}	208.4		206.5	6.9	4.3
E_g	251.8		255.8	1.7	1.4
B_{1g}	286.6				
$A_{1g} + B_{2g}$	289.6	O–Se–O bendings (branches)	288.7	1.7	0.7
	292.9		291.7	4.5	
E_g	300.5		304.2	2.6	2.6
B_{2g}	360.0		360.9	1.9	
E_g	523.0	Se–O stretching (bridging oxygens)	524.5	4.8	4.1
E_g	533.5		532.3	6.7	
A_{1g}	599.6		599.4	5.8	3.5
	617.3				
B_{2g}	713.4		710.2	5.4	3.0
	866.6	Se–O stretching (terminal oxygens)	888.2	−3.9	
A_{1g}	879.5		889.3	−4.1	−4.0
B_{2g}	904.5		912.7	−2.0	−1.0
B_{1g}	936.7		944.1	−0.7	−0.8

The pressure dependencies of Raman modes related to the high-frequency Se–O stretching vibrations do not show any discontinuities or splittings in the entire pressure range studied here (Table 1, Figs. 2 and 3), nor are there any new Se–O bands that would signal a coordination change around the Se atoms. However, the stretching modes of the Se–O bonds in side branches have negative pressure shifts. The weakening of these bands could result from a charge transfer to neighboring interchain bonds (8). As shown in Figs. 2 and 3, several new features appear in the spectra in the bending mode region from 190 to 500 cm^{-1} at pressures between 9 and 11 GPa. These new features are not the missing modes at room temperature and near ambient pressure (Table 1). The band appearing on the low-energy side of the 199.5 cm^{-1} mode has a negative shift up to 18 GPa. In addition, two new modes occur at about 320–340 cm^{-1} between 10 and 11 GPa. Above 7.0 GPa, a new band is visible at 75.8 cm^{-1} in the region of the chain translations. Above about 14 GPa, additional Raman bands are observed in the energy region of the chain deformation and interchain translation modes. All the pressure-induced changes in the Raman spectra are reversible with little hysteresis (Fig. 4).

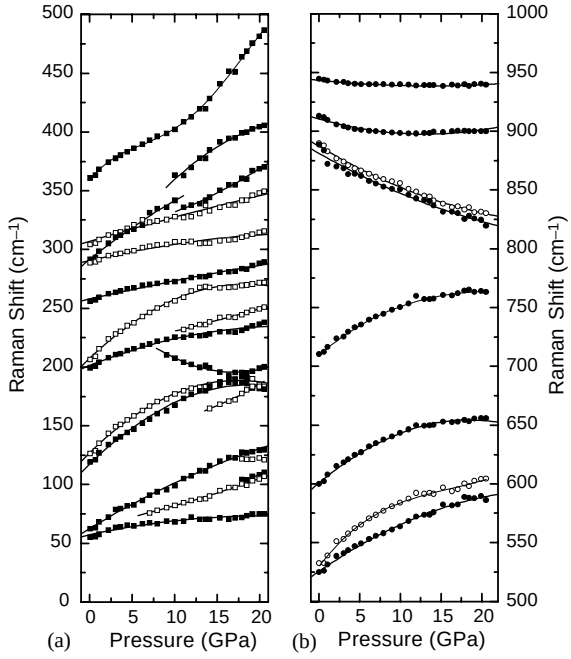

FIG. 3. Pressure dependence of Raman frequencies in SeO_2 upon compression. Lines are guides to the eye.

The appearance of new Raman bands in the 7–11 GPa pressure range indicates a pressure-induced phase transition involving a structural distortion of the low-dimensional SeO_2 structure due to deformations of the chains without changes in both the coordination of the Se atoms and the number of molecular units in the cell. Accordingly, it is possible that the degeneracy of the E_g modes is lifted because the crystal symmetry lowers. Therefore, the splitting of the E_g bands at 53.4, 197.5 and 300.5 cm^{-1} into doublets would imply an orthorhombic distortion of the chain structure, e.g., $D_{4h} \rightarrow D_{2h}(E_g \rightarrow B_{2g} + B_{3g})$ (17). In

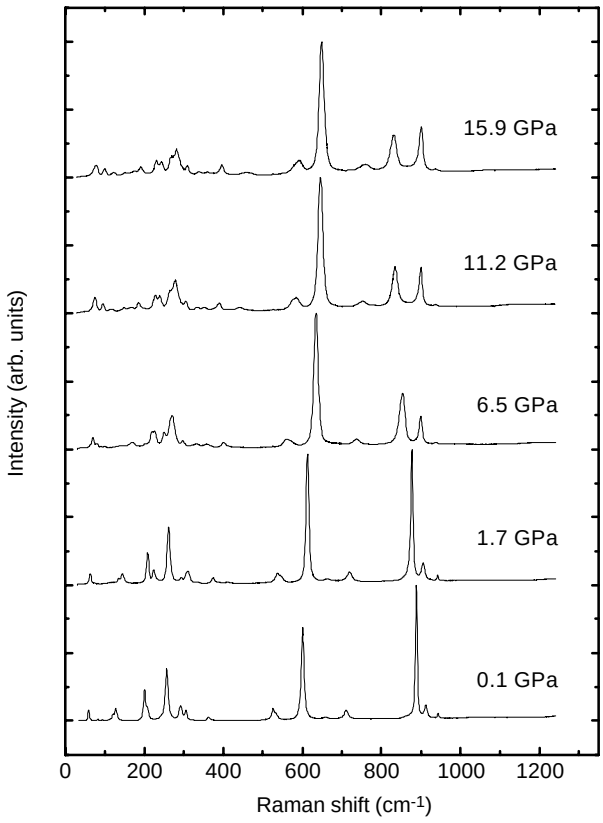

FIG. 4. Selected Raman spectra of SeO_2 upon decompression.

the case of the E_g modes due to Se–O stretchings of the bridging bonds at 523.0 and 533.5 cm^{-1} and to the O–Se–O bending at about 251.8 cm^{-1} (Table 1), splittings are expected. However, they are not resolved as the three bands broaden with increasing pressure.

X-Ray Diffraction

X-ray powder diffraction patterns of SeO_2 upon compression to 23.2 GPa are shown in Fig. 5. Up to about 7.0 GPa, the diagrams can be explained by the $P4_2/mbc$ structural model of selenium dioxide at 286 K and 1 atm (2). At higher pressures, several peaks, initially asymmetric, eventually become well-resolved doublets. Such peak splittings and the appearance of weak additional reflections indicate a structural phase transition with its onset above 7 GPa. It is worth noting that up to about 17 GPa there is only one reflection observed at about $2\theta = 4°$. It is the (110) peak of the $P4_2/mbc$ space group. Upon a further pressure increase, two weak peaks appear in this 2θ range and, overall, the diagrams exhibit significant peak broadening. Prolonged annealing at 425 K did not improve the pattern quality. The reflection broadening could be due not only to pressure gradients in the diamond cell during our experiments, but also to a possible mixture of different SeO_2 phases at these conditions. In fact, most of the observed reflections at the highest pressures can be associated to the peaks already seen at lower pressures.

In order to obtain more detailed information on the high-pressure structural behavior of SeO_2, we refined selected patterns with the Rietveld method included in the GSAS program (13) (Tables 2–5 and Fig. 6). The refined parameters were: the atomic positions, Chebyshev polynomial background, Stephens profile function (14), an overall intensity scaling factor, cell parameters, and March–Dollase preferred orientation correction. The use of the Stephens function (14) for X-ray powder patterns collected at high pressures under non-hydrostatic conditions is discussed in Refs. (15, 16). A similar strategy was employed for all refinements reported in this study. Isotropic thermal parameters ($U_i/U_e * 100$) for the Se, O(1), and O(2) atoms in the $P4_2/mbc$ structural model (2) were fixed at 0.5, 0.7, and 1.0, respectively. These values could be derived from the thermal parameters at ambient pressure and room temperature as given by Ståhl *et al.* (2).

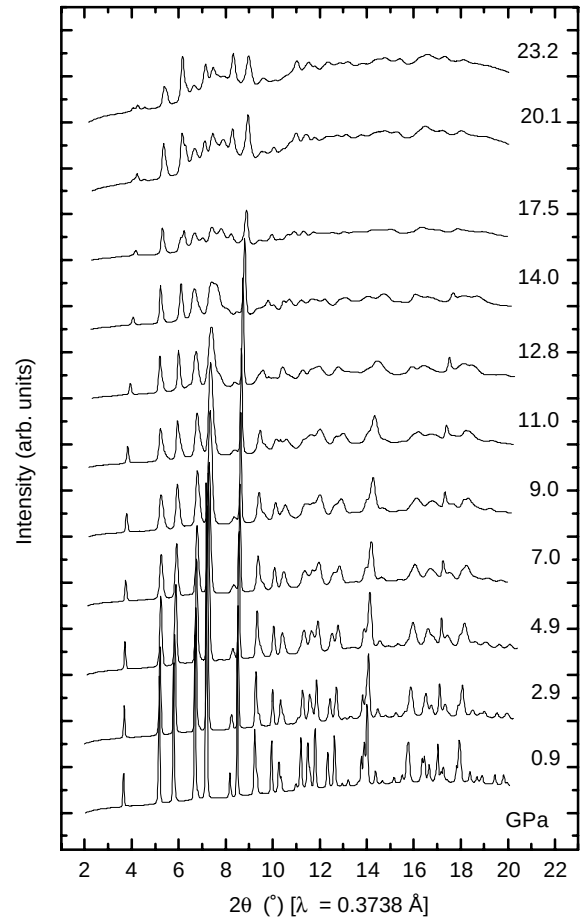

FIG. 5. Selected X-ray powder diffraction patterns of SeO_2 upon compression. Numbers stand for pressures in GPa. The patterns at 14.0 and 23.2 GPa were collected after annealing the sample at 423 K for 8 h.

TABLE 2
Lattice Parameters, Unit Cell Volumes, and Final Atomic Coordinates for SeO_2 at 0.9 and 4.9 GPa—Space Group $P4_2/mbc$, $Z = 8$. Estimated Standard Deviations Are Given in Brackets

			Z0.9 GPa	4.9 GPa
a (Å)			8.2626(2)	8.1463(4)
c (Å)			5.0328(1)	4.9913(2)
V (Å^3)			343.59(1)	331.23(2)
Se	Site	8*h*		
	x		0.1345(2)	0.1337(2)
	y		0.2099(2)	0.2094(2)
	z		0.0	0.0
O(1)	Site	8*g*		
	x		0.1400(6)	0.1372(6)
	y		0.3600(6)	0.3628(6)
	z		$\frac{1}{4}$	$\frac{1}{4}$
O(2)	Site	8*h*		
	x		0.9441(8)	0.9401(9)
	y		0.1710(8)	0.1668(9)
	z		0.0	0.0

Note. Further details of the crystal structure investigation for the phase at 4.9 GPa may be obtained from the Fachinformationzentrum Energie, Physik, Mathematik, D-76344 Eggenstein-Leopoldshafen 2, Germany, http://www.fiz-karlsruhe.de, on quoting the depository number CSD-412233, the names of the authors, and the journal citation.

For the patterns at 0.9 and 4.9 GPa, the input structural model was the one of selenium dioxide at 1 atm and 286 K (2). In this initial model, when adding the second nearest oxygen atoms to the covalently bonded ones in the chains along the *c*-axis, the Se–O coordination can be described as a distorted octahedron. As can be inferred from a comparison of interatomic distances given in Table 3, compression of SeO_2 does not result in a significant decrease in a distortion of the octahedron below 7 GPa. Under the same conditions, the intrachain Se–O distances are independent of pressure within the estimated errors.

The splitting of several reflections and the appearance of weak peaks in the X-ray powder patterns in the pressure range 7–17 GPa (Fig. 5) are indicative of structural distortions in which the number of formula units in the cell is not changed, as seen in the Raman spectra (Figs. 2 and 3). There is no doubling of any axis at the transition. The diagrams collected at this pressure range can no longer be Rietveld refined with the ambient pressure structural model (2). All the new features in the X-ray powder patterns are consistent with the pressure-induced phase transition involving the $P4_2/mbc \rightarrow Pbam$ subgroup relationship, with *Pbam* space group being the *translationengleiche* subgroup of $P4_2/mbc$. Accordingly, in the new structure there are two non-equivalent sites for the Se atoms (4*g* and 4*h*) and three sites for oxygens (8*i*, 4*g*, and 4*h*). The sites 4*g* and 4*h* of *Pbam* are correlated with the site 8*h* of $P4_2/mbc$, while the site 8*i* (*Pbam*) is correlated with the 8*g* one ($P4_2/mbc$). The oxygen atoms at the 4*g* and 4*h* positions are terminal ones while the one at the 8*i*

TABLE 3
Selected Distances (Å) and Angles (deg) in SeO_2 at 0.9 and 4.9 Gpa

		0.9 GPa	4.9 Gpa
Bond distances			
Se–O(1)	(2x)	1.767(3)	1.766(4)
Se–O(2)		1.605(7)	1.615(7)
Shortest interchain distances			
Se–O(2)		2.74	2.69
Se–O(2)	(2x)	2.84	2.79
Bridging angles within chains			
Se–O(1)–Se		122.9(4)	121.5(4)

Note. Estimated standard deviations (ESD) are given in brackets. The distances with no ESD are calculated using the data in Table 1.

TABLE 4
Final Atomic Coordinates for SeO_2 at 9.0 GPa—Space Group *Pbam*, $Z = 8$, $a = 8.134(1)$ Å, $b = 7.928(2)$ Å, $c = 4.9491(3)$ Å, $V = 319.16(8)$ Å^3. Estimated Standard Deviations Are Given in Brackets

Atom	Site	x	y	z
Se(1)	4*g*	0.6316(5)	0.2891(5)	0.0
Se(2)	4*h*	0.2884(4)	0.3607(6)	$\frac{1}{2}$
O(1)	8*i*	0.155(1)	0.405(2)	0.225(2)
O(2)	4*g*	0.441(2)	0.384(2)	0.0
O(3)	4*h*	0.295(2)	0.548(2)	$\frac{1}{2}$

Note. Further details of the crystal structure investigation may be obtained from the Fachinformationzentrum Energie, Physik, Mathematik, D-76344 Eggenstein-Leopoldshafen 2, Germany, http://www.fiz-karlsruhe.de, on quoting the depository number CSD-412234, the names of the authors, and the journal citation.

TABLE 5
Selected Distances (Å) and Angles (deg) in SeO_2 at 9.0 GPa

Bond distances		
Se(1)–O(1)	(2x)	1.91(1)
Se(1)–O(2)		1.72(2)
Se(2)–O(1)	(2x)	1.77(1)
Se(2)–O(3)		1.49(2)
Shortest interchain distances		
Se(1)–O(2)		2.66(2)
Se(1)–O(3)	(2x)	2.85
Se(2)–O(3)		2.57(2)
Se(2)–O(2)	(2x)	2.78
Bridging angles within chains		
Se(1)–O(1)–Se(2)		110.4

Note. Estimated standard deviations (ESD) are given in brackets. The distances with no ESD are calculated from the data in Table 3.

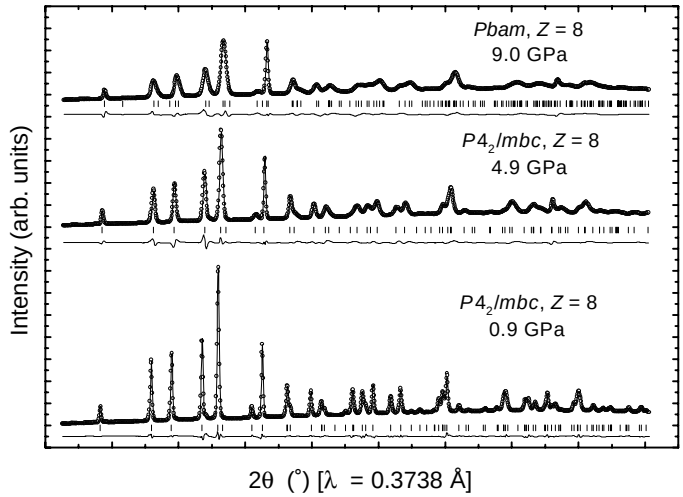

FIG. 6. Observed, calculated, and difference X-ray powder patterns for SeO_2 at selected pressures. Vertical markers indicate Bragg reflections. The residuals $R_{wp}, R_p, R(F^2)$, and χ^2, whose definitions are given in the GSAS manual (13), are—for the diagram at 0.9 GPa: $R_{wp} = 6.4\%$, $R_p = 4.8\%, \chi^2 = 1.58, R(F^2) = 6.3\%$; for the diagram at 4.9 GPa: $R_{wp} = 7.4\%, R_p = 4.6\%, \chi^2 = 1.63, R(F^2) = 8.8\%$; for the diagram at 9.0 GPa: $R_{wp} = 7.7\%, R_p = 5.0\%, \chi^2 = 2.08, R(F^2) = 13.0\%$. All the residuals R_{wp} and R_p are calculated only for the Bragg contribution to the diffraction patterns.

position bridges the chain along the *c*-axis. The starting atomic parameters for the Rietveld refinement of the pattern at 9.0 GPa with the *Pbam* ($Z = 8$) model (Fig. 6) were derived from the final ones in space group $P4_2/mbc$ at 4.9 GPa (Table 2). The thermal parameters for the Se(1) and Se(2) atoms were fixed at 0.5. The O(1), O(2), and O(3) atoms of the same model had their $U_i/U_e * 100$ parameters fixed at 0.7, 1.0, and 1.0, respectively. As can be seen from the data given in Table 5, the octahedral coordination around the Se atoms is still largely distorted in the high-pressure phase. In other words, the nearest and next-nearest oxygen atom neighbors are still distinct. On the other hand, the intrachain Se–O distances vary largely. The magnitude of interchain interactions and chain deformations at high pressures could be evaluated by a comparison of the Se–O–Se intrachain angles (Tables 3 and 5). These angles are much smaller for the distorted *Pbam* structure. It was earlier demonstrated that the effective volume of the *E* pair is approximately the same as the volume taken up by the "O^{2-} ion" (1). The differences in Se–O distances and changes in the angles are the consequence of increased non-bonding interactions between the oxygen atoms and the non-compressible electron lone pair (1) that has to be accommodated in the high-pressure phase.

The symmetry lowering to D_{2h}^9 results in two non-equivalent Se positions (two C_s sites) and three non-equivalent O positions (two C_s sites and one C_1 site). Accordingly, the vibrational modes are distributed (17, 18) as $\Gamma_{vibr.} = 11A_g + 11B_{1g} + 7B_{2g} + 7B_{3g} + 7A_u + 6B_{1u} + 10B_{2u} + 10B_{3u}$, where the A_g, B_{1g}, B_{2g}, and B_{3g} modes are Raman active, while the B_{1u}, B_{2u}, and B_{3u} modes are infrared active. The assignment of the Raman bands in the *Pbam* phase above 7 GPa is made in analogy to the assignment for the ambient pressure structure, when considering separate energy regions for modes due to the Se–O stretchings, O–Se–O bendings, chain deformations and translations (Table 1).

Further structural changes above 17 GPa, involving the appearance of new peaks at low 2θ angles among other new features (Fig. 5), is obscured by broadening of the observed X-ray reflections. However, based on the absence of major overall changes in the X-ray diagrams and Raman spectra, as discussed above, we tend to suggest that there could be a sequence of pressure-induced structural distortions in selenium dioxide up to about 23 GPa, leading to monoclinic symmetry of the structure.

The pressure dependences of lattice parameters, axial ratios, and unit cell volumes across the $P4_2/mbc \rightarrow Pbam$ phase transition up to about 11 GPa are shown in Fig. 7. The ambient pressure lattice parameters from our powder X-ray diffraction data are $a = 8.310(1)$ Å, $c = 5.045(2)$ Å, and $V = 348.39(6)$ Å^3. They are smaller than those determined from single crystal data (2) by 0.6%, 0.3%, and 1.6% relative, respectively. There is no major anomaly in the *c* parameter evolution between 7 and 8 GPa, while the *a* parameter of the low-pressure structure discontinuously splits into *a* and *b* parameters of the *Pbam* space group. The c/a ratio ($P4_2/mbc$) slightly increases indicating the anisotropic axial compression of the chain structure, with the direction along the chain being slightly less compressible. At pressures above 7 GPa it splits into the c/a and c/b ratios of the *Pbam* structure. A change in the pressure dependence of the unit cell volume is clearly noticeable at about 8 GPa at the structural transformation.

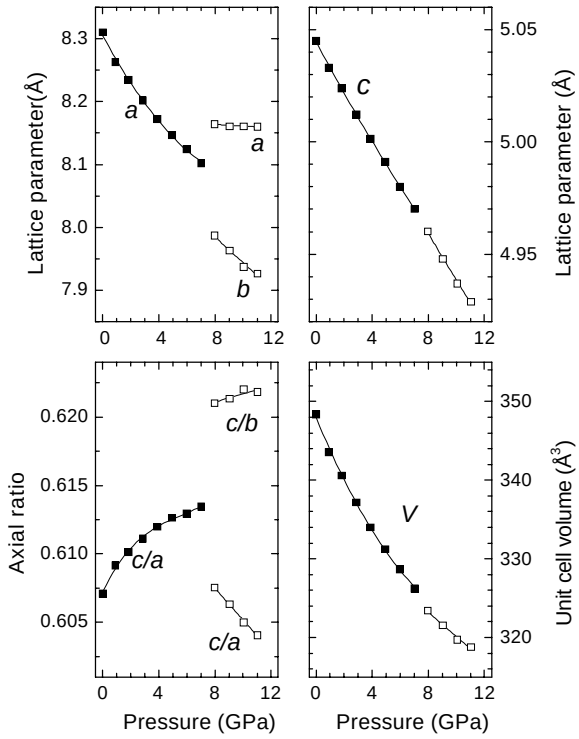

FIG. 7. Pressure dependence of lattice parameters, axial ratios, and unit cell volumes of SeO_2 up at 12 GPa. Open and solid symbols represent the data for the $P4_2/mbc$ ($Z = 8$) and $Pbam$ ($Z = 8$) phases, respectively.

We calculated various Birch–Murnaghan equations of state (EOS) for the compression curve up to 7.0 GPa. The V_0 volume at ambient pressure, K_0 bulk modulus, and K' its first derivative at zero pressure are 348.0(6) Å^3, 75(7) GPa, and 11(2), respectively. The large value of K' can be explained by the low-dimensional character of the crystal structure. When the K' parameter is restricted to 4, K_0 and V_0 are equal to 96(7) GPa and 347.2(9) Å^3, respectively. The extrapolated relative difference of the unit cell volumes between the $P4_2/mbc$ and $Pbam$ phases is about 0.3% at 8 GPa.

Comparison with TeO_2

It is useful to briefly consider the structure and pressure-induced phase transformations in α-TeO_2. In the three-dimensional paratellurite form of TeO_2 ($P4_12_12$, $Z = 4$), tellurium atoms have four neighboring oxygen atoms in a disphenoidal coordination. When the Te electron lone pair (E) or the next-nearest O neighbors are taken into account, the Te–O coordination unit is a distorted TeO_4E bipyramid or a very deformed TeO_6 octahedron, respectively (19). The latter establishes a close structural relationship of α-TeO_2 to the rutile type. Paratellurite undergoes a second-order phase transition to an orthorhombic phase ($P2_12_12_1$, $Z = 4$) at 0.9 GPa and room temperature (19, 20). This reversible transition, involving no volume change, is driven by the soft acoustic mode $\rho V^2 = \frac{1}{2}(C_{11} - C_{12})$ propagating along $\langle 110 \rangle$. The high-pressure phase is a slight distortion of the paratellurite structure. Whether there occur further pressure-induced phase transitions in this material is still a matter of discussion. Based on X-ray powder diffraction data, Liu (21) indicates that there are no additional transformations up to about 25 GPa. On the other hand, Raman scattering data seem to provide evidence for a sequence of phases closely related to the $P2_12_12_1$ one occuring near 4.5 and 11.0 GPa, while the phase forming at about 22.0 GPa is argued to be of the $PbCl_2$ type (22). However, when crystal chemistry of the AX_2 compounds under pressure (23) is considered, the transformation to the cotunnite phase ($Pnam$, $Z = 4$) from rutile-related α-TeO_2 seems to be quite unlikely. The coordination of the cations in the $PbCl_2$ structure is nine and there are several known pressure-induced structures with intermediate coordination numbers from 6 (rutile) to 9, besides the fact that the Te–O coordination unit in α-TeO_2 is in fact a distorted TeO_4E bipyramid.

CONCLUDING REMARKS

The Raman scattering and synchrotron angle-dispersive X-ray diffraction data collected in a diamond cell at room temperature provide evidence for a sequence of pressure-induced phase transitions in SeO_2 involving a structural distortion of the low-dimensional structure due to chain deformations without changes in the coordination of the Se atoms. The transformation occuring above 7.0 GPa is due to a decrease of symmetry to space group $Pbam$ ($Z = 8$). The octahedral coordination around the Se atoms in the new phase remains strongly distorted. Like in the ambient pressure polymorph ($P4_2/mbc$, $Z = 8$) (2), the coordinated polyhedron is a SeO_3E structural unit, where E is a Se lone pair, or an irregular tetrahedron with the O atoms and the Se lone pair at the vertices. A discontinuous change in the pressure dependence of unit cell volumes is observed at this structural transformation. Further structural changes above 17 GPa are likely to be a result of additional distortions in selenium dioxide, resulting in monoclinic symmetry of the structure. All the transformations are reversible with little hysteresis.

The results of this study, evidencing distortions of the chain structure in SeO_2 under pressure without any major structural changes, could be rationalized by recalling the previous work on stereochemistry of elements with electron lone E pairs at atmospheric pressure (1). Galy *et al.* already demonstrated that the effective volume of the E pair is approximately the same as the volume taken up by the "O^{2-} ion". They subsequently discussed the plausible effect of pressure on relevant compounds and suggested that the incomplete coordination spheres around the cations are not condensed at high pressures as a consequence of the

presence of the non-bonded *E* pairs. The behavior of SeO_2 investigated here up to 23 GPa and that of TeO_2 up to 25 GPa, as observed by Liu (21), add much credence to this postulate.

ACKNOWLEDGMENTS

We thank A. Brillante for several fruitful discussions about the Raman scattering experiment and results. L. Farina acknowledges financial support from Max Planck Gesellschaft.

REFERENCES

1. J. Galy, G. Meunier, S. Andersson, and A. Åström, *J. Solid State Chem.* **13,** 142 (1975).
2. K. Ståhl, J. P. Legros, and J. Galy, *Z. Kristallogr.* **202,** 99 (1992).
3. P. Shiv Halasyamani and K. R. Poeppelmeier, *Chem. Mater.* **10,** 2753 (1998).
4. C. Pico, A. Castro, M. L. Veiga, E. Gutierrez-Puebla, M. A. Monge, and C. Ruiz-Valero, *J. Solid State Chem.* **63,** 172 (1986).
5. Y. Porter, N. S. P. Bhuvanesh, and P. Shiv Halasyamani, *Inorg. Chem.* **40,** 1172 (2001).
6. Y. Porter, K. M. Ok, N. S. P. Bhuvanesh, and P. Shiv Halasyamani, *Chem. Mater.* **13,** 1910 (2001).
7. P. Millet, J. Galy, and M. Johnsson, *Solid State Sci.* **1,** 279 (1999).
8. D. Stanila, W. Smith, and A. Anderson, *Spectrosc. Lett.* **33,** 555 (2000).
9. A. Anderson, A. Sanders, and W. Smith, *J. Raman Spectrosc.* **31,** 403 (2000).
10. B. H. Torrie, *Can. J. Phys.* **51,** 610 (1973).
11. A. P. Hammersley, S. O. Svensson, M. Hanfland, A. N. Fitch, and D. Häusermann, *High Pressure Res.* **14,** 235 (1996).
12. H. K. Mao, J. Xu, and P. M. Bell, *J. Geophys. Res.* **91,** 4673 (1986).
13. A. C. Larson and R. B. von Dreele, GSAS: General Structure Analysis System, Los Alamos National Laboratory, 2000.
14. P. W. Stephens, *J. Appl. Crystallogr.* **32,** 281 (1999).
15. A. Grzechnik, A. Vegas, K. Syassen, I. Loa, M. Hanfland, and M. Jansen, *J. Solid State Chem.* **154,** 603 (2000).
16. A. Grzechnik, V. V. Ursaki, K. Syassen, I. Loa, I. M. Tiginyanu, and M. Hanfland, *J. Solid State Chem.* **160,** 205 (2001).
17. E. B. Wilson, J. C. Decius, and P. C. Cross, "Molecular Vibrations." Dover Publications Inc., New York, 1980.
18. L. L. Boyle, *Acta Crystallogr. A* **27,** 76 (1971); L. L. Boyle, *Acta Crystallogr. A* **28,** 172 (1972); L. L. Boyle, *Spectrochim. Acta A* **28,** 1347 (1972); L. L. Boyle, *Spectrochim. Acta A* **28,** 1355 (1972).
19. T. G. Worlton and R. A. Beyerlein, *Phys. Rev. B* **12,** 1899 (1975).
20. P. S. Peercy and I. J. Fritz, *Phys. Rev. Lett.* **32,** 466 (1974); H. Uwe and H. Tokumoto, *Phys. Rev. B* **19,** 3700 (1979); M. Ahart, T. Yagi, and Y. Takagi, *Physica B* **219, 220,** 550 (1996).
21. L.-G. Liu, *J. Phys. Chem. Solids* **48,** 719 (1987).
22. G. A. Kourouklis and A. Jayaraman, *High Pressure Res.* **9,** 23 (1992).
23. J. M. Leger and J. Haines, *Eur. J. Solid State Inorg. Chem.* **34,** 785 (1997).